Geophysical Research Letters

RESEARCH LETTER
10.1029/2022GL100342

Deccan Traps Volcanism Implicated in the Extinction of Non-Avian Dinosaurs in Southeastern China

Mingming Ma[1,2,3], Wenfang Zhang[4], Mengting Zhao[1,3], Yudan Qiu[1,3], Hongming Cai[5], Jiubin Chen[5], and Xiuming Liu[1,3,6]

[1]Key Laboratory of Humid Subtropical Eco-Geographical Process of Ministry of Education, Fujian Normal University, Fuzhou, China, [2]Fujian Provincial Key Laboratory for Subtropical Resources and Environment, Fujian Normal University, Fuzhou, China, [3]College of Geographical Sciences, Fujian Normal University, Fuzhou, China, [4]State Key Laboratory of Lake Science and Environment, Nanjing Institute of Geography and Limnology, Chinese Academy of Sciences, Nanjing, China, [5]School of Earth System Science, Tianjin University, Tianjin, China, [6]Department of Environment and Geography, Macquarie University, Sydney, NSW, Australia

Key Points:

- Hg combined with its isotopic composition indicate the record of Deccan Traps (DT) volcanism
- DT volcanism played an important role in the extinction of non-avian dinosaurs
- The inherent mechanism of how DT caused the mass extinction requires further investigation

Supporting Information:

Supporting Information may be found in the online version of this article.

Correspondence to:

M. Ma, J. Chen and X. Liu,
mamingming159@163.com;
jbchen@tju.edu.cn;
xliu@fjnu.edu.cn

Citation:

Ma, M., Zhang, W., Zhao, M., Qiu, Y., Cai, H., Chen, J., & Liu, X. (2022). Deccan traps volcanism implicated in the extinction of non-avian dinosaurs in southeastern China. *Geophysical Research Letters*, *49*, e2022GL100342. https://doi.org/10.1029/2022GL100342

Received 7 JUL 2022
Accepted 30 NOV 2022

Abstract The extinction of non-avian dinosaurs and its cause(s) have been a matter of debate for several decades. Here we measured Hg and its isotopic composition, heavy metals, and magnetic parameter in a terrestrial basin in southeastern China. Hg exhibited anomalies from 66.4 to 65.6 Ma, with near-zero to positive Δ^{199}Hg values, which reflected the eruption of Deccan Traps (DT) magma. In addition, Hg anomalies coincided with the gradual extinction of non-avian dinosaurs, thereby consistent with the hypothesis that DT played a key role in the mass extinction. Analysis of paleoclimatic records showed that both the Late Maastrichtian warming event (LMWE) and Dan-C2 event occurred at the maxima of the 405-kyr long eccentricity cycle, and the onset of the dinosaur decline was earlier than the LMWE, suggesting that the LMWE played an ancillary role in the mass extinction. The mechanism of how DT caused the mass extinction requires further investigation.

Plain Language Summary The debate concerning the relative importance of the Chicxulub bolide impact and/or Deccan Traps (DT) volcanism as the cause of the extinction of non-avian dinosaurs at the end of the Cretaceous has lasted for several decades. There is lack of direct geological evidence linking the DT eruption with the non-avian dinosaur fossil record, so the Chicxulub bolide impact is regarded by many as the dominant—if not the sole—cause of the mass extinction. Therefore, it is necessary to find new geological evidence to clarify this issue. In this study, the concentration of Hg and its isotope systematics were carefully investigated, combined with palaeontology data and palaeoclimate records, we suggest that DT played a key role in the extinction of non-avian dinosaurs.

1. Introduction

The extinction of non-avian dinosaurs at the end-Cretaceous and its cause(s) are surrounded by controversy due to the extinction process itself, as well as the overlapped occurrences of the Chicxulub bolide impact, Deccan Traps (DT) volcanism, and mass extinction (Schoene et al., 2019; Sprain et al., 2019). There are two views regarding the rapidity of the non-avian dinosaur extinction, according to which the extinction process is considered to be either a) gradual (Z. Zhao et al., 2002, 2017) or b) sudden (Brusatte et al., 2015; Chiarenza et al., 2020; Fastovsky et al., 2004; Pearson et al., 2002). Consequently, two extinction hypotheses have been proposed involving a) DT volcanism (Keller et al., 2018, 2020; Schoene et al., 2019; Z. Zhao et al., 2002), and/or b) the Chicxulub bolide impact (Brusatte et al., 2015; Chiarenza et al., 2020; Pearson et al., 2002). Evidence supporting DT volcanism as the main cause of the mass extinction came from the overlap of the timing of its eruption and the timing of extinction, as well as the environmental degradation caused by the eruption (Keller et al., 2018, 2020; Schoene et al., 2019). However, there is lack of direct geological evidence linking the DT eruption with the non-avian dinosaur fossil record (Burgess, 2019); therefore, the Chicxulub bolide impact is regarded by many as the dominant—if not the sole—cause of the mass extinction (Chiarenza et al., 2020).

To date, most studies have focused on the extinction of non-avian dinosaurs in North America, while adopting stage- or epoch-level time resolutions (Brusatte et al., 2015; Chiarenza et al., 2020; Fastovsky et al., 2004). However, a higher time resolution could reveal a gradual extinction in the Late Maastrichtian (Brusatte et al., 2015; Fastovsky & Sheehan, 2005; Pearson et al., 2002; S. C. Wang & Dodson, 2006). Therefore, given the ambiguity of North American records, it is necessary to find other terrestrial deposits with accurate age estimates and

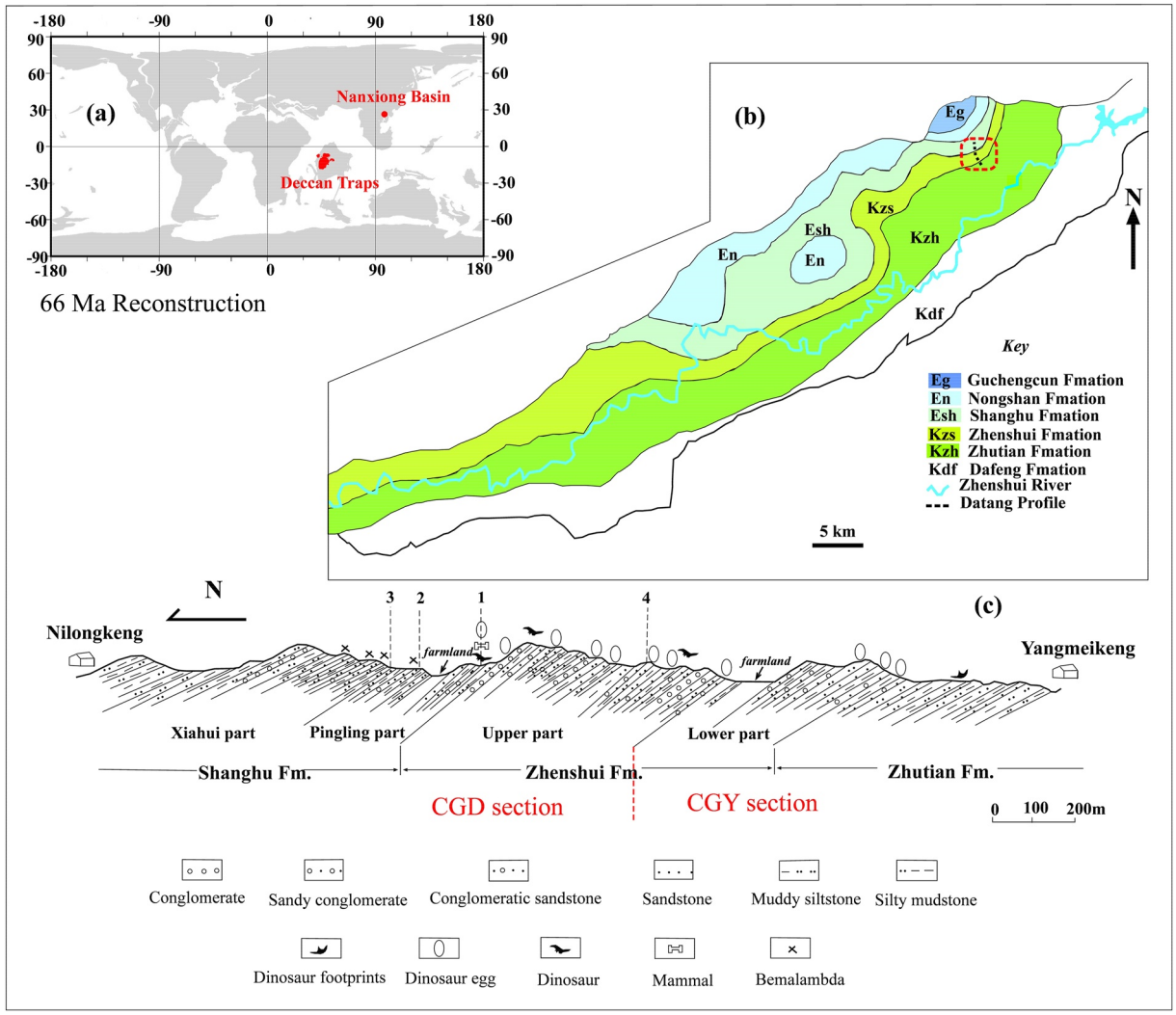

Figure 1. Sample location and relative geological background. (a) Paleogeographic reconstruction at 66 Ma (from https://www.odsn.de/odsn/services/paleomap/paleomap.html); (b) geological map of the Nanxiong Basin (modified from G. Li et al. [2010]); (c) stratigraphy, fossil records, and four proposed K–Pg boundaries (numbers 1–4) of the Datang section (modified from X. Zhang et al. [2006]). CGD section, Chinese–German Datang section; CGY section, Chinese–German Yuanpu section.

higher time resolution (Brusatte et al., 2015; Fastovsky et al., 2004). The terrestrial basin (i.e., Nanxiong Basin; Figure 1) of southeastern China is an ideal place for investigating these issues. Earlier paleontological investigations in this basin revealed a large number of fossils, including dinosaur footprints, dinosaur eggs, and mammals. Though the fossils here are not as abundant as in North America, compared to the Williston and Powder River Basins, the thickness of the stratum recording the extinction of non-avian dinosaurs exceeds 100 m. Paleomagnetic chronology revealed that the 100-m thick stratum spans only ~0.4 Myr (Clyde et al., 2010) (Figure S1 in Supporting Information S1), and could be correlated with the 20–40 m section spanning the Maastrichtian portion of chron C29r in the Williston Basin (Sprain et al., 2018). Furthermore, an additional stratum with thickness exceeding 60 m was apparent between the dinosaur extinction and the subsequent expansion of large mammals (i.e., Bemalambda) (Z. Zhao et al., 2002, 2017). Here, we carefully investigated the concentration of Hg and its isotope systematics, together with palaeontology data and palaeoclimate records from the Nanxiong Basin, to reveal (a) the record of DT volcanism in the study area; and (b) the linkage between DT volcanism and the non-avian dinosaur extinction process as well as the delayed radiation of mammals.

2. Geological Setting and Methods

2.1. Geological Setting

The Nanxiong Basin is in southeastern China (Figure 1a); it is elongated with its axis oriented from north-east to south-west (Figure 1b). Continuous red fluvial–lacustrine clastics spanning from the Upper Cretaceous to the Lower Paleocene are preserved in the basin. A large number of palaeontology, chronology, and palaeoclimate studies have been conducted (Clyde et al., 2010; Ma et al., 2018, 2021; Y. Wang, 2012; X. Zhang et al., 2006; Z. Zhao et al., 2002, 2017); hence, the basin is an ideal location for producing global continental K–Pg boundary profiles (Nichols & Johnson, 2008). The CGD-CGY section (also called Datang section) consists of three formations, from bottom to top (Figure 1c): the Zhutian formation (i.e., muddy siltstone and silty mudstone; 105.0 m in thickness), the Zhenshui formation (i.e., silty mudstone with sandstone and conglomerate interbeds: 295.5 m in thickness), and the Shanghu formation (i.e., muddy siltstone and silty mudstone; 288.3 m in thickness). The sediments are rich in paleontological fossils (Figure 1c): dinosaur footprints were found in the Zhutian formation, a large number of dinosaur and dinosaur eggs were found in the Zhenshui formation, dinosaur and mammal fossils coexisted in the bottom layer of the Shanghu formation, while abundant large mammal (i.e., Bemalambda) fossils were found in the middle and upper parts of the Shanghu formation. Four K–Pg boundaries were proposed according to the different criteria (Figure 1c); however, more evidence (Figure S2 in Supporting Information S1) has led to the suggestion that the K–Pg boundary was at the bottom part of the Shanghu formation (i.e., boundary 1 in Figure 1c) (Clyde et al., 2010; Ma et al., 2018, 2021; Y. Wang, 2012; M. Zhao et al., 2021).

2.2. Methods

In order to minimize the effect of lithology changes, the samples were mainly selected from muddy siltstone or silty mudstone. Fresh samples were air-dried in the laboratory, and then multiple-proxy analysis, such as magnetic susceptibility (χ), Hg concentration and its isotope systematics, carbon isotope, major element and heavy metal concentrations were conducted. A detailed description of relative analysis in this study is given in Supporting Information S1.

3. Results

3.1. Hg Concentration and Isotopes

Earlier studies have revealed that Hg is concentrated in sediments rich in organic matter, clay minerals, or sulphides; therefore, Hg concentrations should be normalized by their dependencies (Font et al., 2016; Grasby et al., 2019; Shen et al., 2020). In the Nanxiong Basin, very low total organic carbon (TOC) values (i.e., <0.2 wt%, while most being <0.1 wt%) were reported (M. Zhao et al., 2021); such low TOC values are unsuitable for Hg normalization (Grasby et al., 2019; Shen et al., 2020). Generally, for terrestrial sediments, Hg was hosted by clay minerals (Shen, Yu, et al., 2019). Therefore, in this study, Hg concentrations were normalized to the Al_2O_3 concentration (Figure 2c). The Hg and Hg/Al_2O_3 contents of the Zhutian formation and the lower part of the Zhenshui formation were at a relatively low level, which subsequently increased significantly from the upper part of the Zhenshui formation to the Pingling part of the Shanghu formation. These Hg anomalies were confirmed by repeated measurements (Figure S3 in Supporting Information S1). Within the Xiahui part of the Shanghu formation, concentrations declined to values comparable to those of the Zhutian formation and the lower part of the Zhenshui formation. Isotopically, Δ^{199}Hg ranged from −0.09 to 0.16‰ (Figure 2d): it exhibited negative values in the Zhutian formation and the lower part of the Zhenshui formation, an increase to near-zero or even positive values with minor fluctuations from the Zhenshui formation until the Pingling part of the Shanghu formation, and a decrease to negative values again in the Xiahui part of the Shanghu formation. δ^{202}Hg ranged from −3.28 to −0.95‰ (Figure 2e) and anticorrelated with Δ^{199}Hg.

3.2. Heavy Metals

Similar to Hg, heavy metals were also generally hosted by clay minerals in sediments, so their concentrations were normalized to Al_2O_3. Co, Cd, and pollution load indices exhibited trends similar to the Hg trend (Figures 2f, 2g, and 2h), with relatively low levels in the Zhutian formation and the lower part of the Zhenshui formation, and significantly increased levels from the upper part of the Zhenshui formation to the Pingling part of the Shanghu

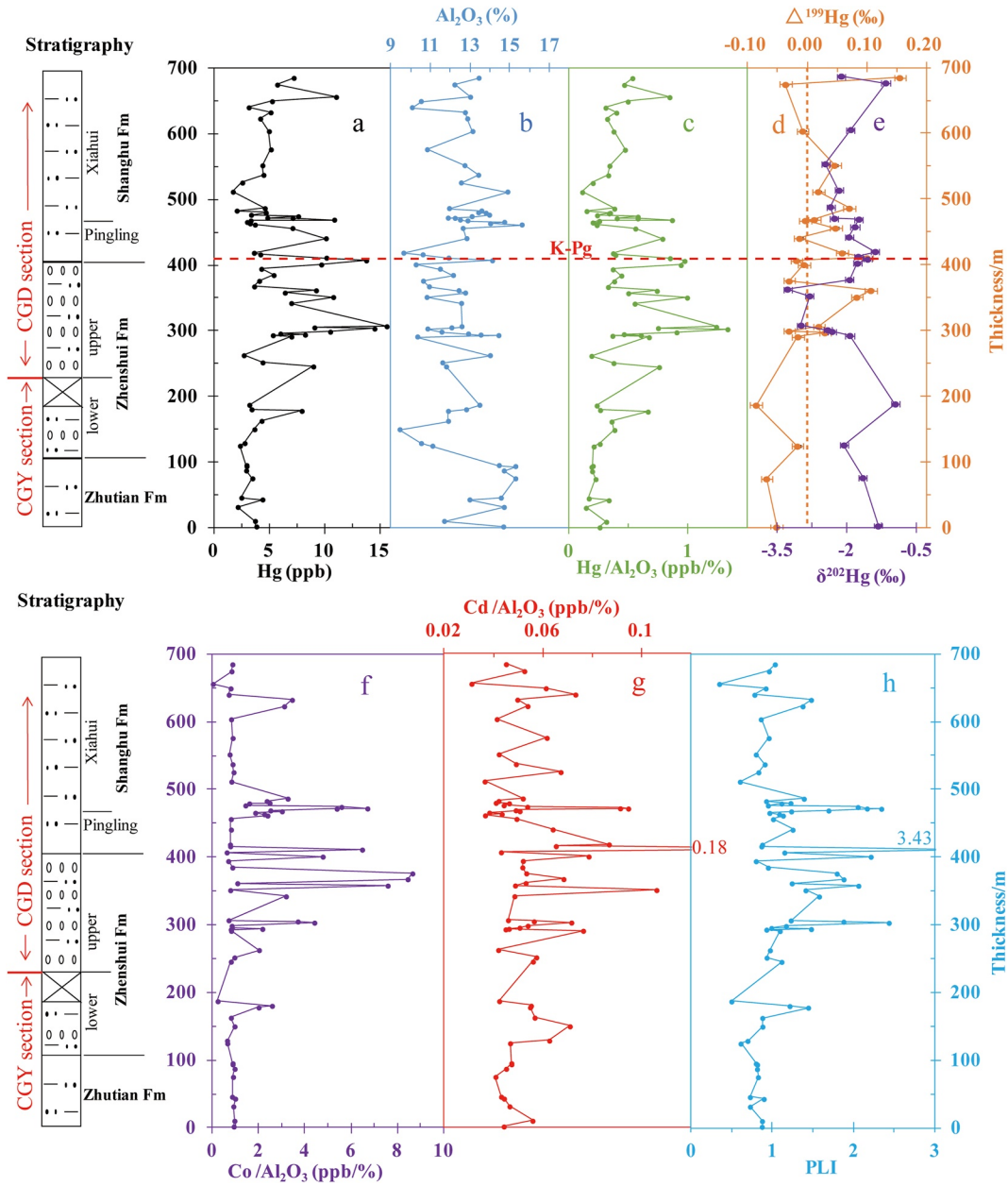

Figure 2. Stratigraphy, and (a) total Hg concentration, (b) Al_2O_3, (c) Hg/Al_2O_3 ratio, (d) $\Delta^{199}Hg$, (e) $\delta^{202}Hg$, (f) Co/Al_2O_3, (g) Cd/Al_2O_3, and (h) pollution load indices of the CGD-CGY section. The lithologies in the stratigraphic section is described in the legend on Figure 1c.

formation with clear fluctuations. Within the Xiahui part of the Shanghu formation, concentrations of Co and Cd declined again, with values comparable to those in the Zhutian formation and lower part of the Zhenshui formation.

3.3. Magnetic Susceptibility (χ) and Carbon Isotope ($\delta^{13}C_{carb}$)

χ ranged from 2×10^{-8} to 12×10^{-8} m^3 kg^{-1} (Figure 3b), with fluctuations consistent with our earlier results (Ma et al., 2018, 2021), while exhibiting high values around ~66.2 and ~65.7 Ma; in particular, double peaks were apparent around ~65.7 Ma. The new $\delta^{13}C_{carb}$ data in this study were consistent with previous results, with significant negative excursions around ~66.2 and ~65.7 Ma (Figure 3c). The 405-kyr filtered χ exhibited

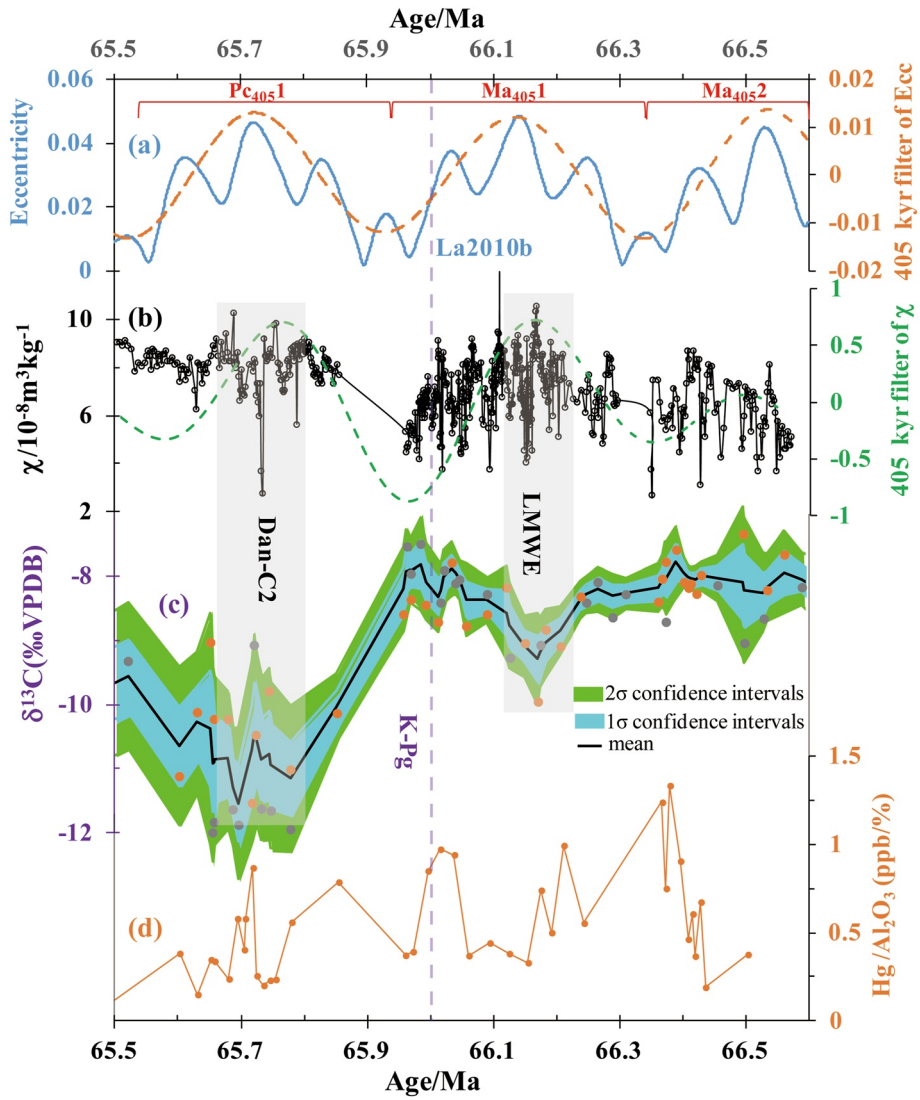

Figure 3. (a) La2010b orbital solution (Laskar et al., 2011) (blue) and filtered by long eccentricity (405-kyr) illustrated in orange dash line; (b) χ curve (black) and filtered by long eccentricity (405-kyr) illustrated in green dash line; (c) $\delta^{13}C$ record of pedogenic carbonates, gray circles represent the results from Clyde et al. (2010) and Y. Wang (2012), while orange circles from this study; (d) Hg/Al_2O_3 ratio. LMWE: Late Maastrichtian warming event; Dan-C2: Dan-C2 event (Quillévéré et al., 2008).

significant periodicity, which corresponded well to the 405-kyr filter of the orbital solution curve of La2010b (Laskar et al., 2011) (Figure 3a). Moreover, wavelet analysis was also conducted for the χ record using the Acycle software (M. Li et al., 2019), which conforms the 405-kyr periodicity (Figure S4 in Supporting Information S1). There were also significant non-405 kyr cycles (probably precession) in the χ record (Figure S4 in Supporting Information S1), likely due to the coverage of farmland (Figure 1c) that affected the stability of these cycles, resulting in discontinuity of the profile.

4. Discussion

4.1. Record of Deccan Traps Volcanism in the Nanxiong Basin

Volcanic activity was the most prominent source of atmospheric Hg prior to the Anthropocene (Shen, Algeo, et al., 2019). Large amounts of gaseous Hg (0) and Hg (II) can be emitted during large igneous province (LIP) eruptions. As Hg (0) in the atmosphere has 0.5–2.0 years residence time, it can be distributed globally,

subsequently converts to Hg (II) through oxidation, and can deposit in sediments by wet and dry precipitation (Grasby et al., 2019). Significant Hg spikes have been found in many marine (Font et al., 2016, 2018; Keller et al., 2018, 2020; Sial et al., 2016) and terrestrial (Fendley et al., 2019; Gu et al., 2022; S. Li et al., 2022; Percival et al., 2018) K–Pg sections worldwide and have been attributed to the DT LIP eruption. In addition to Hg, other volatile heavy metals (including Co, Pb, Ni, As, and Cd) can also be released during LIP events and deposited with fly ash (Grasby et al., 2015, 2019). In this study, the Hg, Co, and Cd anomalies before and after the K–Pg boundary (Figure 2) could be related to the LIP events.

Volcanism is not the sole source of Hg and other metals; other sources may also contribute to their budgets. Therefore, we cannot attribute the Hg anomalies to volcanic activity based only on Hg concentrations (Grasby et al., 2019). Earlier studies have shown that Hg isotopes, especially the mass independent fractionation of ^{199}Hg (Odd-MIF), is another promising proxy for tracing the Hg source, as it is principally triggered by photoreaction, rather than other surface biochemical processes (Blum et al., 2014). During photoreactions, Hg (II) is reduced to Hg (0) and returns to the atmosphere, thereby resulting in negative and positive Δ^{199}Hg in the products and residual reactant, respectively (Blum et al., 2014). For instance, negative Δ^{199}Hg is observed in soil, terrestrial sediments, and land plants, while positive Δ^{199}Hg is observed in precipitation, aquatic organisms, and atmospheric particles. Volcanic eruptions exhibit Δ^{199}Hg typically close to zero (Shen, Algeo, et al., 2019; Yin et al., 2016), the post-emissional transport would, however, induce positive Δ^{199}Hg values for Hg emitted from volcanoes due to photolysis reactions. In this case, the near zero Δ^{199}Hg would indicate the deposition of Hg that undergone less photoreduction during the trajectory from volcanic emission to deposition, while highest value would imply some Hg had undergone a relatively intensive photolysis. Anyway, both cases should be accompanied by Hg enrichment. Therefore, increased Hg concentrations, combined with Odd-MIF, have been widely used to trace ancient volcanic activities (Grasby et al., 2019; Shen, Algeo, et al., 2019; Sial et al., 2016). Generally, there are two Hg sources in terrestrial sediments: atmospheric deposition and terrestrial input through erosion. Figure 2 shows negative Δ^{199}Hg values in the Zhutian formation and the lower part of the Zhenshui formation, indicating a typical terrestrial signature. However, near zero to positive values from the Zhenshui formation to the Pingling part of the Shanghu formation, combined with Hg enrichment, could be attributed to the supply of atmospheric Hg derived from volcanic Hg (0) (with near zero Δ^{199}Hg) or atmospheric Hg (II) (with positive Δ^{199}Hg) (Chen et al., 2012; Rolison et al., 2013). The decrease to negative values again in the Xiahui part of the Shanghu Formation, with decreased Hg concentration, likely indicates increased terrestrial Hg contribution; therefore, the dominant Hg source changed from terrestrial to atmospheric and again to terrestrial (Figure 2 and Figure S5a in Supporting Information S1). Although near zero and even positive Δ^{199}Hg values obtained for samples at depth of 124 and 684 m, respectively, but they cannot be identified as volcanic in origin because of the lack of increased Hg concentrations. δ^{202}Hg was controlled by different pathways than Δ^{199}Hg, including hydrothermal reactions, sorption/deposition, and diagenesis (Blum et al., 2014), the anticorrelation between Δ^{199}Hg and δ^{202}Hg (Figure 2 and Figure S5b in Supporting Information S1) could be caused by the Hg supply change, as the atmospheric Hg (II) particulates have typically relatively higher Δ^{199}Hg and lower δ^{202}Hg values, while atmospheric Hg (0) has typically relatively lower Δ^{199}Hg and higher δ^{202}Hg values (Blum et al., 2014). This was also found in a terrestrial Permian–Triassic boundary section (i.e., Lubei, South China Craton), which was attributed to the supply of volcanic Hg (Shen, Yu, et al., 2019).

The Hg and pollution load indices anomalies lasted approximately 0.8 Myr (i.e., 66.4–65.6 Ma; Figure 4). Two phases of local volcanic activity were discovered in the basin: (a) 96 ± 1 Ma based on the basalt age in the central Zhutian formation (Shu et al., 2004), and (b) ∼60 Ma based on a thin volcanic ash layer in the central Nongshan formation (Tong et al., 2013), both of which are inconsistent with the Hg anomalies. Although intense volcanic activity, represented by the widespread occurrence of volcanic strata, occurred during the Lower Cretaceous in South China, the red strata basin formed during the Upper Cretaceous, indicating the termination of volcanic activities and the beginning of sedimentation (X. Li et al., 2019). High-precision geochronology has previously demonstrated that the majority of the DT eruption occurred in less than 1 Myr (U–Pb dating: 66.3–65.5 Ma (Schoene et al., 2019); ^{40}Ar-^{39}Ar dating: 66.413–65.422 Ma (Sprain et al., 2019)). Therefore, the persistence of Hg and pollution load indices anomalies is consistent with the DT eruption period.

4.2. Linkage Between Deccan Traps Volcanism and the Non-Avian Dinosaur Extinction

Previous studies revealed that non-avian dinosaurs from two parallel K–Pg sections in Nanxiong Basin exhibiting a clear gradual extinction (Figure S6 in Supporting Information S1), indicating the importance of DT

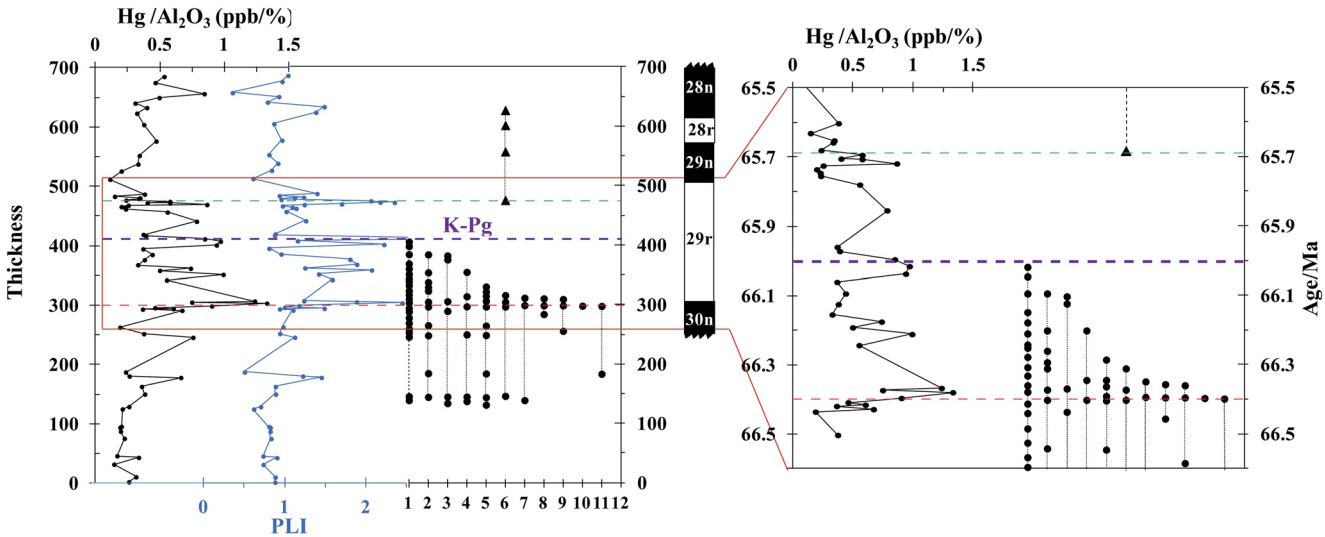

Figure 4. Hg/Al_2O_3 ratio, pollution load indices, and the stratigraphic occurrence of dinosaur eggs (indicated by black circles) and Bemalambda (indicated by black triangles). Numbers 1–11 represent different oospecies of dinosaur egg (1: *Macroolithus yaotunensis*; 2: *Elongatoolithus elongatus*; 3: *Macroolithus rugustus*; 4: *Elongatoolithus sp.*; 5: *Elongatoolithus andrewsi*; 6: *Apheloolithus shuinanensis*; 7: *Prismatoolithus hukouensis*; 8: *Stromatoolithus pinglingensis*; 9: *Ovaloolithus cf. O. laminadermus*; 10: *Ovaloolithus cf. O. chinkangkouensis*; 11: *Nanshiungoolithus chuetienensis*, modified from Z. Zhao et al. [2002]). The red dashed line represents the layer (age) at which the dinosaurs began to disappear, the purple dashed line represents the K–Pg boundary, the green dashed line represents the layer (age) of the expansion of Bemalambda.

volcanism (Z. Zhao et al., 2002, 2017). Here, we provide direct evidence confirming the hypothesis: Figure 4 shows that the beginning of the non-avian dinosaur extinction corresponds to the increase in Hg and pollution load indices at ~66.4 Ma, which is the beginning of the majority DT volcanic activity (i.e., 66.300–66.413 Ma (Schoene et al., 2019; Sprain et al., 2019)). An increasing number of dinosaurs disappeared with the continued volcanic activity, while no dinosaurs survived beyond the K–Pg boundary, indicating that the ultimate extinction of non-avian dinosaurs corresponded to the highest eruption-volume period (Schoene et al., 2019) or the acceleration (Sprain et al., 2019) of DT volcanism. Although non-avian dinosaurs went extinct, DT volcanism and Hg anomalies continued. The expansion of large mammals, represented by Bemalambda, occurred after the end of the Hg and pollution load indices anomalies (Figure 4), consistent with the hypothesis that the DT volcanic activity not only caused the extinction of non-avian dinosaurs but also delayed the radiation of mammals in the basin (Z. Zhao et al., 2002, 2017).

Our earlier work demonstrated that χ and $\delta^{13}C_{carb}$ are effective proxies for paleoclimatic reconstruction in the study area, and two hyperthermals (i.e., Late Maastrichtian warming event (LMWE) and Dan-C2) were identified (Ma et al., 2018, 2021; M. Zhao et al., 2021). The high-resolution χ and $^{13}C_{carb}$ further confirmed these two hyperthermals: χ peaks corresponded with negative $\delta^{13}C_{carb}$ excursions (Figure 3), moreover, the carbonate isotope excursions of this study consistent with the marine record (Figure S7 in Supporting Information S1). Earlier studies demonstrated that the hyperthermals (except for the LMWE and Paleocene–Eocene thermal maximum (PETM), i.e., PETM) during the Late Cretaceous–Early Eocene were mainly controlled by the orbital forcing of eccentricity (Barnet et al., 2019) and occurred during the maxima of the 405-kyr cycle. Here, analysis of the χ curve showed that Dan-C2 and the LMWE maxima were all within the maxima of the 405-kyr eccentricity cycle (Figure 3b and Figure S4 in Supporting Information S1), consistent with the recent work from Zumaia, Spain (Gilabert et al., 2021), suggesting the orbital forcing control. However, the total duration of the onset, peak and recovery of LMWE (~200–300 kyr, Figure S7 in Supporting Information S1) is significantly longer than a typical orbitally forced hyperthermal (~100 kyr). This implies that an additional forcing mechanism, such as the CO_2 emissions released by DT volcanic activity during the LMWE, cannot be excluded (Barnet et al., 2019; Keller et al., 2018, 2020; Schoene et al., 2019; L. Zhang et al., 2018).

Earlier studies suggested that the LMWE played an important role in the mass extinction at the end of Cretaceous (Keller et al., 2018, 2020; Schoene et al., 2019); however, the onset of the dinosaur decline (i.e., ~66.4 Ma) occurred earlier than this warming event (Figures 3 and 4). In addition, though the LMWE was stronger than

other hyperthermals in the Paleocene and early Eocene (such as Dan-C2; Figure S7 in Supporting Information S1), it was definitely weaker than the PETM during which no mass extinction occurred, indicating that the LMWE is not the primary trigger for the elevated extinction (Hull et al., 2020). Previous work observed decrease of average values of dinosaur eggshell thickness and the gradually increased number and proportion of pathologic eggshells in the Nanxiong Basin (Z. Zhao et al., 2002), implying that the normal reproduction of dinosaurs was severely disturbed, eventually leading to extinction. This seems to be consistent with the Hg anomalies, as well as the Co and Cd enrichments in sediments (Figures 2 and 4) and the records of enriched trace elements in dinosaur eggshells (Z. Zhao et al., 2002). However, the quantity and rate of these toxic substances released by DT eruptions was still unclear. Take Hg for example, an estimated 99.3–177.8 Mt Hg was emitted into the atmosphere based on Hg/SO_2 ratio (Font et al., 2016), while the Hg/S ratio was estimated from modern volcanoes, with a 20-fold value range of $0.02–0.4 \times 10^{-14}$ (Nriagu, 1989). Recently, an Hg flux of 500–3,000 Mg yr^{-1} was estimated during the pulsed eruptions each lasted less than 1,000 years (Fendley et al., 2019), this was similar with present-day anthropogenic emissions (~2,000 Mg yr^{-1} (Obrist et al., 2018)), which was not enough to cause mass extinction. While the results of Fendley et al. (2019) was based on global mercury box model that probably contains many uncertainties for K–Pg interval Hg flux calculation. In addition to heavy metals, volcanic activities emit a large amount of toxic gases, including SO_2 and H_2S. SO_2 and H_2S contribute to the formation of acid rain, which accelerates the deterioration of the biosphere, as speculated in K-Pg sections from Gubbio (Italy), Bidart (France), Zumaia (Spain), and Elles (Tunisia) (Font et al., 2016, 2018; Keller et al., 2020). Fendley et al. (2019) suggested that Deccan eruptions released enough SO_2 to cause repeated 1–6°C cooling each lasted less than 1,000 years, but till now no reliable paleoclimate record was available due to the short cooling period. Therefore, considering the uncertainties of Hg flux estimation and the lack of reliable records of deteriorative climatic/environmental conditions caused by the toxic substances, the inherent mechanism how DT caused the mass extinction requires further investigation.

5. Conclusion

In conclusion, the Hg, Co and Cd concentrations exhibited anomalies from approximately 66.4 to 65.6 Ma (Figures 2 and 4). $\Delta^{199}Hg$ exhibited near zero to positive values in the layers with increased Hg concentration (Figure 2), consistent with the DT volcanic Hg supply. The Hg and other heavy metals anomalies were also consistent with the hypotheses that the DT volcanism was associated with the gradual extinction of non-avian dinosaurs (Figure 4). Analysis of the χ curve showed that the LMWE maxima were within the maxima of the 405-kyr eccentricity cycle (Figure 3), and the onset of the dinosaur decline was earlier than the LMWE (Figures 3 and 4). Though our records suggest that DT played a key role in the extinction of non-avian dinosaurs, more work is needed to illustrate the inherent mechanism of how DT caused the mass extinction.

Data Availability Statement

All of the data have been deposited and made available at: https://doi.org/10.5281/zenodo.6808913.

Acknowledgments
The authors appreciate the constructive comments from Dr. James Barnet and the anonymous reviewers. This research was supported by the National Science Foundation of China (Grants: 42277440, 42130507, 41625012, 41830647, and 41961144028), and IGCP Project 679.

References

Barnet, J., Littler, K., Westerhold, T., Kroon, D., Leng, M. J., Bailey, I., et al. (2019). A high-Fidelity benthic stable isotope record of late Cretaceous–early Eocene climate change and carbon-cycling. *Paleoceanography and Paleoclimatology*, *34*(4), 672–691. https://doi.org/10.1029/2019PA003556

Blum, J. D., Sherman, L. S., & Johnson, M. W. (2014). Mercury isotopes in Earth and environmental sciences. *Annual Review of Earth and Planetary Sciences*, *42*(1), 249–269. https://doi.org/10.1146/annurev-earth-050212-124107

Brusatte, S. L., Butler, R. J., Barrett, P. M., Carrano, M. T., Evans, D. C., Lloyd, G. T., et al. (2015). The extinction of the dinosaurs. *Biological Reviews*, *90*(2), 628–642. https://doi.org/10.1111/brv.12128

Burgess, S. (2019). Deciphering mass extinction triggers. *Science*, *363*(6429), 815–816. https://doi.org/10.1126/science.aaw0473

Chen, J. B., Hintelmann, H., Feng, X. B., & Dimock, B. (2012). Unusual fractionation of both odd and even mercury isotopes in precipitation from Peterborough, ON, Canada. *Geochimica et Cosmochimica Acta*, *90*, 33–46. https://doi.org/10.1016/j.gca.2012.05.005

Chiarenza, A. A., Farnsworth, A., Mannion, P. D., Lunt, D. J., Allison, P. A., & Morgan, J. V. (2020). Asteroid impact, not volcanism, caused the end-Cretaceous dinosaur extinction. *Proceedings of the National Academy of Sciences of the United States of America*, *117*(29), 17084–17093. https://doi.org/10.1073/pnas.2006087117

Clyde, W. C., Ting, S., Snell, K. E., Bowen, G. J., Tong, Y., Koch, P. L., et al. (2010). New paleomagnetic and stable-isotope results from the Nanxiong Basin, China: Implications for the K/T boundary and the timing of Paleocene mammalian turnover. *The Journal of Geology*, *118*(2), 131–143. https://doi.org/10.1086/649893

Fastovsky, D. E., Huang, Y., Hsu, J., Martin-McNaughton, J., Sheehan, P. M., & Weishampel, D. B. (2004). Shape of Mesozoic dinosaur richness. *Geology*, *32*(10), 877–880. https://doi.org/10.1130/G20695.1

Fastovsky, D. E., & Sheehan, P. M. (2005). The extinction of the dinosaurs in North America. *Geological Society of America Today*, *15*(3), 4–10. https://doi.org/10.1130/1052-5173(2005)152.0.CO;2

Fendley, I. M., Mittal, T., Sprain, C. J., Marvin-DiPasquale, M., Tobin, T. S., & Renne, P. R. (2019). Constraints on the volume and rate of Deccan Traps flood basalt eruptions using a combination of high-resolution terrestrial mercury records and geochemical box models. *Earth and Planetary Science Letters*, *524*, 115721. https://doi.org/10.1016/j.epsl.2019.115721

Font, E., Adatte, T., Andrade, M., Keller, G., Bitchong, A. M., Carvallo, C., et al. (2018). Deccan volcanism induced high-stress environment during the Cretaceous–Paleogene transition at Zumaia, Spain: Evidence from magnetic, mineralogical and biostratigraphic records. *Earth and Planetary Science Letters*, *484*, 53–66. https://doi.org/10.1016/j.epsl.2017.11.055

Font, E., Adatte, T., Sial, A. N., Lacerda, L. D., Keller, G., & Punekar, J. (2016). Mercury anomaly, Deccan volcanism, and the end-Cretaceous mass extinction. *Geology*, *44*(2), 171–174. https://doi.org/10.1130/G37451.1

Gilabert, V., Batenburg, S. J., Arenillas, I., & Arz, J. A. (2021). Contribution of orbital forcing and Deccan volcanism to global climatic and biotic changes across the Cretaceous-Paleogene boundary at Zumaia, Spain. *Geology*, *50*(1), 21–25. https://doi.org/10.1130/G49214.1

Grasby, S. E., Beauchamp, B., Bond, D., Wignall, P., Talavera, C., Galloway, J. M., et al. (2015). Progressive environmental deterioration in Northwestern Pangea leading to the latest Permian extinction. *The Geological Society of America Bulletin*, *127*(9–10), 9–10. https://doi.org/10.1130/B31197.1

Grasby, S. E., Them, T. R., Chen, Z., Yin, R., & Ardakani, O. H. (2019). Mercury as a proxy for volcanic emissions in the geologic record. *Earth-Science Reviews*, *196*, 1–16. https://doi.org/10.1016/j.earscirev.2019.102880

Gu, X., Zhang, L., Yin, R., Grasby, S. E., Yao, H., Tan, J., & Wang, C. (2022). Deccan volcanic activity and its links to the end-Cretaceous extinction in Northern China. *Global and Planetary Change*, *210*, 103772. https://doi.org/10.1016/j.gloplacha.2022.103772

Hull, P. M., Bornemann, A., Penman, D. E., Henehan, M. J., Norris, R. D., Wilson, P. A., et al. (2020). On impact and volcanism across the Cretaceous-Paleogene boundary. *Science*, *367*(6475), 266–272. https://doi.org/10.1126/science.aay5055

Keller, G., Mateo, P., Monkenbusch, J., Thibault, N., Punekar, J., Spangenberg, J. E., et al. (2020). Mercury linked to Deccan Traps volcanism, climate change and the end-Cretaceous mass extinction. *Global and Planetary Change*, *194*, 103312. https://doi.org/10.1016/j.gloplacha.2020.103312

Keller, G., Mateo, P., Punekar, J., Khozyem, H., Gertsch, B., Spangenberg, J., et al. (2018). Environmental changes during the Cretaceous-Paleogene mass extinction and Paleocene-Eocene thermal maximum: Implications for the Anthropocene. *Gondwana Research*, *56*, 69–89. https://doi.org/10.1016/j.gr.2017.12.002

Laskar, J., Fienga, A., Gastineau, M., & Manche, H. (2011). La2010: A new orbital solution for the long-term motion of the Earth. *Astronomy & Astrophysics*, *532*, A89. https://doi.org/10.1051/0004-6361/201116836

Li, G., Hirano, H., Batten, D. J., Wan, X. Q., Willems, H., & Zhang, X. Q. (2010). Biostratigraphic significance of spinicaudatans from the Upper Cretaceous Nanxiong group in Guangdong, South China. *Cretaceous Research*, *31*(4), 387–395. https://doi.org/10.1016/j.cretres.2010.05.003

Li, M., Hinnov, L., & Kump, L. (2019). Acycle: Time-series analysis software for paleoclimate research and education. *Computers & Geosciences*, *127*, 12–22. https://doi.org/10.1016/j.cageo.2019.02.011

Li, S., Grasby, S. E., Zhao, X., Chen, J., Zheng, D., Wang, H., et al. (2022). Mercury evidence of Deccan volcanism driving the latest Maastrichtian warming event. *Geology*, *50*(10), 1140–1144. https://doi.org/10.1130/G50016.1

Li, X., Zhang, C., Li, Y., Wang, Y., & Liu, L. (2019). Refined chronostratigraphy of the late Mesozoic terrestrial strata in South China and its tectono-stratigraphic evolution. *Gondwana Research*, *66*, 143–167. https://doi.org/10.1016/j.gr.2018.09.006

Ma, M., He, M., Zhao, M. T., Peng, C., & Liu, X. M. (2021). Evolution of atmospheric circulation across the Cretaceous–Paleogene (K–Pg) boundary interval in low-latitude East Asia. *Global and Planetary Change*, *199*, 103435. https://doi.org/10.1016/j.gloplacha.2021.103435

Ma, M., Liu, X., & Wang, W. (2018). Palaeoclimate evolution across the Cretaceous–Palaeogene boundary in the Nanxiong Basin (SE China) recorded by red strata and its correlation with marine records. *Climate of the Past*, *14*(3), 287–302. https://doi.org/10.5194/CP-14-287-2018

Nichols, D. J., & Johnson, K. R. (2008). *Plants and the KT boundary*. Cambridge University Press

Nriagu, J. O. (1989). A global assessment of natural sources of atmospheric trace metals. *Nature*, *338*(6210), 47–49. doi https://doi.org/10.1038/338047a0

Obrist, D., Kirk, J. L., Zhang, L., Sunderland, E. M., Jiskra, M., & Selin, N. E. (2018). A review of global environmental mercury processes in response to human and natural perturbations: Changes of emissions, climate, and land use. *Ambio*, *47*(2), 116–140. https://doi.org/10.1007/s13280-017-1004-9

Pearson, D. A., Schaefer, T., Johnson, K. R., Nichols, D. J., & Hunter, J. P. (2002). *Vertebrate biostratigraphy of the hell creek formation in Southwestern North Dakota and Northwestern South Dakota* (pp. 145–167). Geological Society of America Special Paper.

Percival, L. M. E., Jenkyns, H. C., Mather, T. A., Dickson, A. J., Batenburg, S. J., Ruhl, M., et al. (2018). Does large igneous province volcanism always perturb the mercury cycle? Comparing the records of Oceanic Anoxic Event 2 and the end-Cretaceous to other Mesozoic events. *American Journal of Science*, *318*(8), 799–860. https://doi.org/10.2475/08.2018.01

Quillévéré, F., Norris, R. D., Kroon, D., & Wilson, P. A. (2008). Transient ocean warming and shifts in carbon reservoirs during the early Danian. *Earth and Planetary Science Letters*, *265*(3–4), 600–615. https://doi.org/10.1016/j.epsl.2007.10.040

Rolison, J. M., Landing, W. M., Luke, W., Cohen, M., & Salters, V. J. M. (2013). Isotopic composition of species-specific atmospheric Hg in a coastal environment. *Chemical Geology*, *336*, 37–49. https://doi.org/10.1016/j.chemgeo.2012.10.007

Schoene, B., Eddy, M. P., Samperton, K. M., Keller, C. B., Keller, G., Adatte, T., & Khadri, S. F. R. (2019). U-Pb constraints on pulsed eruption of the Deccan Traps across the end-Cretaceous mass extinction. *Science*, *363*(6429), 862–866. https://doi.org/10.1126/science.aau2422

Shen, J., Algeo, T. J., Planavsky, N. J., Yu, J., Feng, Q., Song, H., et al. (2019). Mercury enrichments provide evidence of Early Triassic volcanism following the end-Permian mass extinction. *Earth-Science Reviews*, *195*, 191–212. https://doi.org/10.1016/j.earscirev.2019.05.010

Shen, J., Feng, Q., Algeo, T. J., Liu, J., Zhou, C., Wei, W., et al. (2020). Sedimentary host phases of mercury (Hg) and implications for use of Hg as a volcanic proxy. *Earth and Planetary Science Letters*, *543*, 116333. https://doi.org/10.1016/j.epsl.2020.116333

Shen, J., Yu, J., Chen, J., Algeo, T. J., Xu, G., Feng, Q., et al. (2019). Mercury evidence of intense volcanic effects on land during the Permian-Triassic transition. *Geology*, *47*(12), 1117–1121. https://doi.org/10.1130/G46679.1

Shu, L. S., Deng, P., Wang, B., Tan, Z. Z., Yu, X. Q., & Sun, Y. (2004). Lithology, kinematics and geochronology related to Late Mesozoic basin-mountain evolution in the Nanxiong-Zhuguang area, South China. *Science in China—Series D: Earth Sciences*, *47*(8), 673–688. https://doi.org/10.1360/03yd0113

Sial, A., Chen, J., Lacerda, L., Frei, R., Tewari, V., Pandit, M., et al. (2016). Mercury enrichment and Hg isotopes in Cretaceous–Paleogene boundary successions: Links to volcanism and palaeoenvironmental impacts. *Cretaceous Research*, *66*, 60–81. https://doi.org/10.1016/j.cretres.2016.05.006

Sprain, C. J., Renne, P. R., Clemens, W. A., & Wilson, G. P. (2018). Calibration of chron C29r: New high-precision geochronologic and paleomagnetic constraints from the Hell Creek region, Montana. *GSA Bulletin*, *130*(9–10), 1615–1644. https://doi.org/10.1130/b31890.1

Sprain, C. J., Renne, P. R., Vanderkluysen, L., Pande, K., Self, S., & Mittal, T. (2019). The eruptive tempo of Deccan volcanism in relation to the Cretaceous-Paleogene boundary. *Science*, *363*(6429), 866–870. https://doi.org/10.1126/science.aav1446

Tong, Y. S., Li, Q., & Wang, Y. Q. (2013). An introduction to recent advance in the study of the continental Early Paleogene stages in China (in Chinese with English abstract). *Journal of Stratigraphy*, *37*, 428–440. https://doi.org/10.0253/4959(2013)04-0428.13

Wang, S. C., & Dodson, P. (2006). Estimating the diversity of dinosaurs. *Proceedings of the National Academy of Sciences*, *103*(37), 13601–13605. https://doi.org/10.1073/pnas.0606028103

Wang, Y. (2012). *Paleoclimate changes of the Late Cretaceous-Late Paleocene in the Nanxiong Basin*. Nanjing University. (in Chinese with English abstract).

Yin, R., Feng, X., Hurley, J. P., Krabbenhoft, D. P., Lepak, R. F., Hu, R., et al. (2016). Mercury isotopes as proxies to identify sources and environmental impacts of mercury in sphalerites. *Scientific Reports*, *6*(1), 1–8. https://doi.org/10.1038/srep18686

Zhang, L., Wang, C. S., Wignall, P. B., Kluge, T., Wan, X. Q., Wang, Q., & Gao, Y. (2018). Deccan volcanism caused coupled pCO_2 and terrestrial temperature rises, and pre-impact extinctions in Northern China. *Geology*, *46*(3), 271–274. https://doi.org/10.1130/G39992.1

Zhang, X., Lin, J. N., Li, G., & Ling, Q. X. (2006). Non-marine Cretaceous-Paleogene boundary section at Datang of Nanxiong, northern Guangdong (in Chinese with English abstract). *Journal of Stratigraphy*, *30*(4), 327–340. https://doi.org/10.0253/4959(2006)04.0327.14

Zhao, M., Ma, M., He, M., Qiu, Y., & Liu, X. (2021). Evaluation of the four potential Cretaceous-Paleogene (K–Pg) boundaries in the Nanxiong Basin based on evidences from volcanic activity and paleoclimatic evolution. *Science China Earth Sciences*, *64*(4), 631–641. https://doi.org/10.1007/s11430-020-9736-0

Zhao, Z., Mao, X. Y., Chai, Z. F., Yang, G. C., Kong, P., Ebihara, M., et al. (2002). A possible causal relationship between extinction of dinosaurs and K/T iridium enrichment in the Nanxiong Basin, South China: Evidence from dinosaur eggshells. *Palaeogeography, Palaeoclimatology, Palaeoecology*, *178*(1–2), 1–17. https://doi.org/10.1016/S0031-0182(01)00361-3

Zhao, Z., Ye, J., & Wang, Q. (2017). Dinosaur extinction and subsequent mammalian recovery during the Cretaceous-Paleogene (K/Pg) transition in the Nanxiong Basin (in Chinese with English abstract). *Chinese Science Bulletin*, *62*(17), 1869–1881. https://doi.org/10.1360/N972016-00886

References From the Supporting Information

Barnet, J., Littler, K., Kroon, D., Leng, M. J., Westerhold, T., Röhl, U., & Zachos, J. C. (2017). A new high-resolution chronology for the late Maastrichtian warming event: Establishing robust temporal links with the onset of Deccan volcanism. *Geology*, *46*(2), 147–150. https://doi.org/10.1130/g39771.1

Buck, B. J., Hanson, A. D., Hengst, R. A., & Shu-sheng, H. (2004). "Tertiary dinosaurs" in the Nanxiong Basin, Southern China, are reworked from the Cretaceous. *The Journal of Geololy*, *112*(1), 111–118. https://doi.org/10.1086/379695

Chen, J. B., Hintelmann, H., & Dimock, B. (2010). Chromatographic pre-concentration of Hg from dilute aqueous solutions for isotopic measurement by MC-ICP-MS. *Journal of Analytical Atomic Spectrometry*, *25*(9), 1402–1409. https://doi.org/10.1039/c0ja00014k

Gradstein, F. M., Ogg, J. G., Schmitz, M. D., & Ogg, G. M. (2012). *The geologic time scale 2012*. Cambridge University Press.

Huang, Q., Chen, J., Huang, W., Reinfelder, J. R., Fu, P., Yuan, S., et al. (2019). Diel variation in mercury stable isotope ratios records photoreduction of $PM_{2.5}$-bound mercury. *Atmospheric Chemistry and Physics*, *19*(1), 315–325. https://doi.org/10.5194/acp-19-315-2019

Huang, Q., Liu, Y., Chen, J., Feng, X., Huang, W., Yuan, S., et al. (2015). An improved dual-stage protocol to pre-concentrate mercury from airborne particles for precise isotopic measurement. *Journal of Analytical Atomic Spectrometry*, *30*(4), 957–966. https://doi.org/10.1039/C4JA00438H

Kroon, D., & Zachos, J. C. (2007). Leg 208 synthesis: Cenozoic climate cycles and excursions. In D. Kroon, J. C. Zachos, & C. Richter (Eds.), *Prsoceedings of the Ocean Drilling Program, Scientific Results* (Vol. *208*, pp. 1–55). https://doi.org/10.2973/odp.proc.sr.208.201.2007

Ling, Q. X., Zhang, X. Q., & Lin, J. N. (2005). New advance in the study of the Cretaceous and Paleogene strata of the Nanxiong Basin (in Chinese with English abstract). *Journal of Stratigraphy*, *29*, 596–601. https://doi.org/10.0253/4959(2005)ZK.0596.06

Signor, P. W., & Lipps, J. H. (1982). Sampling bias, gradual extinction patterns, and catastrophes in the fossil record. In L. T. Silver & P. H. Schultz (Eds.), *Geological implications of impacts of large asteroids and comets on Earth* (pp. 291–296). Geological Society of America Special Paper.

Wu, H., Zhang, S., Jiang, G., Hinnov, L., Yang, T., Li, H., et al. (2013). Astrochronology of the Early Turonian–Early Campanian terrestrial succession in the Songliao Basin, northeastern China and its implication for long-period behavior of the solar system. *Palaeogeography, Palaeoclimatology, Palaeoecology*, *385*, 55–70. https://doi.org/10.1016/j.palaeo.2012.09.004

Zhang, X. Q. (1984). Division and biota of the Luofozhai group in pingling section, Nanxiong Basin (in Chinese with English abstract). *Journal of Stratigraphy*, *8*, 239–254.

Zhang, X. Q. (1992). A study on ostracod fauna of Shanghu Formation and Cretaceous-Tertiary boundary in Nanxiong Basin, Guangdong (in Chinese with English abstract). *Acta Palaeontologica Sinica*, *31*, 678–702.

Zhang, X. Q., & Li, G. (2015). Discussion on geological age of the Pingling Member of Shanghu Formation in the Nanxiong Basin, Guangdong province (in Chinese with English abstract). *Journal of Stratigraphy*, *39*, 74–80.

Zhang, Y. Y., Chen, J. B., Zheng, W., Sun, R. Y., Yuan, S. L., Cai, H. M., et al. (2020). Mercury isotope compositions in large anthropogenically impacted Pearl River, South China. *Ecotoxicology and Environmental Safety*, *191*, 110229. https://doi.org/10.1016/j.ecoenv.2020.110229

Zhao, Z. K., Ye, J., Li, H. M., Zhao, Z. H., & Yan, Z. (1991). Extinction of the dinosaurs across the Cretaceous-Tertiary boundary in Nanxiong Basin, Guandong Province. *Certebrata Palasiatica*, *29*(1), 1.